substance: boron compounds with group IV elements
property: properties of boron-silicon compounds

General literature: [70E2, 79L]

Thermodynamic analysis of complex boron-silicon systems [91E2].

Boron-rich side of the B-Si phase diagram and structure parameters, enthalpy [81A].

Preparation and study of the electrical properties of Si-B alloys with a high boron concentration [81D] (for details see LB III/41C "Boron", section "doped β-rhombohedral boron")

Microstructure and thermoelectric properties of arc-melted silicon borides SiB_n [97C].

Thermodynamic analysis of the complex boron-silicon system including the quaternary B-Si-C-N systems and B-Si-O-C systems in [91E1, 91E2].

$Si_{11}B_{31}$

Preparation [79L], crystalline structure [79L]

$SiB_{2.89}$

α-rhombohedral boron structure group with the restriction that in this case the relatively large Si atoms substitute for icosahedral boron atoms as well. Compared with the other representatives of this structure group, this considerably enlarges the unit cell volume (see Fig. 1 [93B]).

lattice parameters
(in Å)

a	6.319	*T* = 300 K	X-ray diffraction	62M,
c	12.713			91L
c/*a*	2.01			
V	439.6 $Å^3$			
a	6.3483	*T* = 300 K	X-ray diffraction	89T
c	12.7382			
c/*a*	2.01			
a	6.3221(7)	*T* = 300 K	arc melted	94L
c	12.712(2)			
a	6.3378(3)	*T* = 300 K	sintered	
c	12.747(9)			

interatomic distances
(in Å)

d	1.71	inter-icosahedral	91L
	1.95	intra-icosahedral	
	1.76	origin to 6 B(1)	
	1.95	origin to 6 B(2)	
	2.47	X – X (chain)	
	2.00	X – 3 B(1)	

Density of states calculation of the idealized structure $Si_4B_{10} = (B_{12}Si_2)(Si_2)$ in Fig. 2 [90B].

SiB_3

Preparation [77M1, 70E2], crystalline structure [77M1, 77M2]

SiB_3 is composed of twelve-atom, distorted icosahedra and two-atom, intericosahedral chains [97A, 98A2]. According to the lattice parameters this compound must probably be attributed to the before-mentioned compound $SiB_{2.89}$.

SiB_3 was not found to be stable in either circumstance. Rather, it is a metastable phase whose formation is driven by the relative ease of its nucleation and growth. The Si boride that exists in stable equilibrium with boron-saturated Si is SiB_6. A qualitative understanding of the metastability of SiB_3 comes from recognizing the conflict between the bonding requirements of icosahedral borides such as SiB_3 and the size mismatch between Si and B atoms [98A2].

lattice parameters

a	6.32 Å	*T* = 300 K	X-ray diffraction	98A2
c	12.71 Å			

For details of structure and comparison with other representatives of the α-rhombohedral boron structure group see [98A2].

Raman spectrum in Fig. 3 [97A].

Association of broad icosahedral Raman bands with the substitutional disorder compared with boron carbide [98A1].

$Si_{1-x}B_x$ films

Plasma deposited films; temperature dependence of the Peltier energy in Fig. 4 [80P]; temperature dependence of the activation energy of the electrical conductivity in Fig. 5. [80P].

Temperature dependence of the density of states $N(E)$, the electrical conductivities $\sigma(E, 400K)$, and $\sigma(E, T)f(1-f)$ vs. hole energy for the $x_g = 0.17$ film with $W_A = 0.1$ eV (WA defined by $\mu(E, T) = \mu(E)\exp(W_A/k_BT)$) in Fig. 6 [80P].

Analysis of thermopower and conductivity for mixed band and broad tail state conduction in [80P].

SiB_4

lattice: rhombohedral (boron-carbide type) [70E2; 77M1]; space group: D_{3d}^5 – R $\bar{3}$ m.

lattice parameters
(hexagonal presentation)

a	6.35 Å	*T* = 300 K	X-ray diffraction	61C
c	12.69 Å			

resistivity

ρ	1.75 Ω cm	*T* = 293 K	polycrystal	65M, 77M1

thermal conductivity

κ	5.9(5) W m^{-1} K^{-1}	*T* = 100°C	polycrystal	79B
	4.7(4) W m^{-1} K^{-1}	*T* = 500°C		
	3.5(3) W m^{-1} K^{-1}	*T* = 1000°C		

density

d	2.41 g cm^{-3}	T = 300 K	X-ray	61C
	2.44 g cm^{-3}	T = 300 K	pycnometric	77M1

melting point

T_m	1269°C			70E3, 77M1

coefficient of linear thermal expansion

α_{av}	6·10^{-6} K^{-1}	T = 20...1000°C	polycrystal, α_{av}: average value	79B

microhardness

H_K	2000...2500 kg mm^{-2}	T = 300 K	Knoop hardness	64S
	1870...2290 kg mm^{-2}	T = 300 K	Knoop hardness	60R, 77M1

For temperature dependence, see [79B].

Young's modulus

E	2800 Pa	T = 300 K		79B

SiB_6

lattice: orthorhombic [70E2, 77M1, 81A]

lattice parameters
(in Å)

a	14.392	T = 300 K	X-ray diffraction	58A,
b	18.267			77M1,
c	9.8852			81A
a	14.89	T = 300 K	X-ray diffraction	87W
b	18.96			
c	9.31...9.91			

For dependence on composition and temperature, see [79L].

The unit cell consists of approximately 280 atoms [81A]. The major elements of the structure are (i) fifteen-atom clusters, icosihexahedra, which contain both Si and B atoms; (ii) twelve-atom, boron-rich icosahedral clusters; (iii) individual, tetrahedrally coordinated Si atoms [59K, 79A, 86V]. SiB_6 melts incongruently, to β-rhombohedral boron and a liquid, at about 1850 °C [81A, 59K, 79A].

Preparation by hot pressing in [87W].

resistivity

ρ	0.5...20 Ω cm	T = 300 K	hot-pressed	87W
	0.2 Ω cm	T = 300 K	polycrystal	61C, 77M1

Temperature dependence of the resistivity in Fig. 7 [87W].

Temperature dependence of the Hall effect data in Fig. 8 [87W].

Temperature dependence of the thermoelectric power in Fig. 9 [87W].

Raman spectrum of amorphous SiB_6 in Fig. 10 [80L].

density

d	2.39 g cm^{-3}	T = 300 K	X-ray	58A
	2.43 g cm^{-3}	T = 300 K	pycnometric	77M1

melting point

T_m	1864°C			70E3, 77M1

volume expansion coefficient

β	18.15·10^{-6} K^{-1}	T = 20...1190°C	a decreases, b and c increase with increasing temperature	79L

microhardness

H_K	3200...3500 kg mm^{-2}	T = 300 K	Knoop hardness	64S
	2520...2870 kg mm^{-2}			60R, 77M1

SiB_{12}

Preparation [77M1, 70E2], crystalline structure [77M1]

B–Si compounds of undefined structure (possibly SiB_{14} structure)

Compositions $Si_xM_{1-x}B_{\approx 30}$ (M = Fe, Co, Ni); (cp. $FeB_{29.5}$).

resistivity: Fig. 16

thermoelectric power: Fig. 17.

n-type conductivity character at low, p-type at high temperatures [81D].

SiB_{14}

Structure

The crystalline structure has been suggested to be isotypic with β-rhombohedral boron (see vol 17e, section 8.1). It is based on a nearly cubic closest-packed arrangement of B_{84} units. Additionally a (B_7Si_3)–Si–(B_7Si_3) group is expected to be arranged along the trigonal axis of the rhombohedral cell (i.e. the crystallographic c-axis) [70M1, 70M2, 77M2].

lattice parameters
(hexagonal presentation)

a	11.13 Å	T = 300 K	X-ray diffraction	65G,
c	23.83 Å			70M1

Physical properties

conductivity

σ	6·10^{-6} Ω^{-1} cm^{-1}	T = 300 K	For temperature dependence, see Fig. 11.	78D, 78P2, 78P3, 79P

resistivity

ρ	60...7.6·10^4 Ω cm	T = 300 K	For temperature dependence, cf. Fig. 16.	76A

thermoelectric power

S	+ 400 μV K^{-1}	T = 300 K	For temperature dependence, see Fig. 12.	78D, 78P3, 79P
	40...340 μV K^{-1}	T = 300 K	For temperature dependence, cf. Fig. 17.	76A

mobility

$\mu_{H,p}$	< 1 cm^2/V s	T = 300 K	Hall mobility	76A

p-type conductivity character of pure material [79P, 76A].

trap level

a dominating trapping level similar to β-rhombohedral boron exists

E_t	0.38 eV		trapping level	78P2, 79P

dielectric constants: see Figs. 13...15

thermal conductivity

κ	0.015...0.03 W cm^{-1} K^{-1}	T = 300 K		76A

density

d	2.48 g cm^{-3}	T = 300 K	experimental	76A
	2.51 g cm^{-3}	T = 300 K	X-ray	76A

The transport properties are strongly influenced by impurities.

$SiB_{\approx 36}$

Interstitially doped β-rhombohedral boron; see LB III/41C (boron).

Amorphous Si–B alloys

The amorphous films are prepared by radio frequency plasma decomposition of silane-diborane gas mixtures [79T]. The films are hydrogenated.

Physical properties

The energy gaps of films with zero Si content and zero B content (Fig. 18) are considerably greater than those of sputtered a-Si (1.34 eV) and a-B (1.1 eV). This is attributed to the high Si–H and B–H bond energy.

Optical gap and electrical activation energy: Fig. 18

g-value: Fig. 19

electrical conductivity: Fig. 20

spin density: Fig. 21

absorption edge: Fig. 22

IR transmission: Fig. 23.

References:

58A Adamsky, R.: Acta Crystallogr. 11 (1958) 744.
59K Knarr, W.A.: PhD Thesis (1959) .
60R Rizzo, M. F., Bidwell, L. R.: J. Am. Ceram. Soc. 43 (1960) 550.
61C Colton, E.: Mater. Des. Eng. 53 (1961) 9.
62M Magnusson, B., Brosset, C.: Acta Chem. Scand. 16 (1962) 449.
63F Feigelson, R.S., Kingery, W.D.: Am. Ceram. Soc. Bull. 42 (1963) 688.
64S Samsonov, G. V., Sleptsov, V. M.: Proshk. Metall. 6 (1964) 58.
65G Giese, R. F. Jr., Economy, J., Matkovich, V. I.: Z. Kristallogr. 122 (1965) 144.
65M Meerson, G. A., Kiparisov, S. S., Ourevich, M. A.: Proshk. Metall. 3 (1965) 32.
70E1 Boron 3, T. Niemyski, ed., PWN Warsaw, 1970
70E2 Ettmayer, P., Horn, H. C., Schwetz, K. A.: Microchim. Acta Suppl. IV (1970) 87.
70E3 Elliot, R. P.: Metallurgia, 1970.
70M1 Matkovich, V. I., Economy, J.: see [70E1] p. 167.
70M2 Matkovich, V. I., Economy, J.: see [70E1] p. 159.
76A Armas, B., Combescure, C., Dusseau, J. M., Lepetre, I. P., Robert, J. L., Pistoulet, B.: J. Less-Common Met. 47 (1976) 135.
77B Berezin, A. A., Golikova, O. A., Zaitsev, V. R., Kazanin, M. M., Orlov, V. M., Tkalenko, E. N., in:Boron and Refractory Borides, (Matkovich V. 1., ed.) Springer: Berlin, Heidelberg, New York 1977, p. 52.
77M1 Makarenko, G. N.: see [77B], p. 310.
77M2 Matkovich, V. I., Economy, J.: see [77B], p. 96.
78D Dusseau, J. M., Ensuque, L., Im-Sareoun, Lepetre, T. P.: Phys. Status Solidi (a) 47 (1978) K 11.
78P1 Pistoulet, B., Robert, J. L., Dusseau, J. M., Roche, F. M., Girard, P., in: Physics of Semiconductors (Edinburgh Conf.), 1978, p. 793.
78P2 Pistoulet, B., Robert, J. L., Dusseau, J. M., Ensuque, L.: J. Non-Cryst. Solids 29 (1978) 29.
78P3 Pistoulet, B., Robert, J. L., Dusseau, J. M.: see [78P1], p. 1009.
79A Arabei, B.G.: Neorg. Mater. 15 (1979) 1589.
79B Bairamashvili, I. A., Kalandadze, G. I., Eristavi, A. M., Jobava, J. Sh., Chotulidi, V. V., Saloev, Yu. I.: J. Less-Common Met. 67 (1979) 455.
79L Lugscheider, F., Reimann, H., Quadakkers, W. J.: Ber. Dtsch. Keram. Ges. 56 (1979) 301.
79P Pistoulet, B., Robert, J. L., Dusseau, J. M., Roche, F., Girard, P., Ensuque, L.: J. Less-Common Met. 67 (1979) 131.
79T Tsai, C. C.: Phys. Rev. B. 19 (1979) 2041.
80L Lannin, J.S., Messier, R.: Phys. Rev. Lett. 45 (1980) 1119.
80P Persans, P.: J. Non-Cryst. Solids 35+36 (1980) 369.
81A Armas, B., Malé, G., Salanoubat, D., Chatillion, C., Allibert, M.: J. Less-Common Met. 82 (1981) 245. (Proc. 7th Int. Symp. Boron, Borides and Rel. Compounds, Uppsala, Sweden, 1981).
81D Dusseau, J.M., Robert, J.L., Armas, B., Combescure, C.: J. Less-Common Met. 82 (1981) 137 (Proc. 7th Int. Symp. Boron, Borides and Rel. Compounds, Uppsala, Sweden, 1981).
86V Vlasse, M., Slack, G.A., Garbauskas, M., Kasper, J.S., Viala, J.C.: J. Solid State Chem. 63 (1986) 31.
87W Wood, C., Emin, D., Feigelson, R.S., Mackinnon, I.D.R.: in: Novel Refractory Semiconductors, MRS Symp. Proc. Vol. 97, D. Emin, T.L. Aselage, C. Wood ed., Materials Research Soc.: Pittsburgh, 1987, p. 33.
89T Tremblay, R., Angers, R.: Ceram. Int. 15 (1989) 73.
90B Bullett, D.W.: in: The Physics and Chemistry of Carbides, Nitrides and Borides; NATO ASI Series E: Applied Sciences Vol. 185, R. Freer ed., Kluwer Academic Publishers: Dordrecht, 1990, p. 513.
91E1 Eristavy, V.Yu.: in: Boron-Rich Solids, Proc. 10th Int. Symp. Boron, Borides and Rel. Compounds, Albuquerque, NM 1990 (AIP Conf. Proc. 231), D. Emin, T.L. Aselage, A.C. Switendick, B. Morosin, C.L. Beckel ed., American Institute of Physics: New York, 1991, p. 436.

91E2 Eristavy, D.V., Mindin, V.Yu: in: Boron-Rich Solids, Proc. 10th Int. Symp. Boron, Borides and Rel. Compounds, Albuquerque, NM 1990 (AIP Conf. Proc. 231), D. Emin, T.L. Aselage, A.C. Switendick, B. Morosin, C.L. Beckel ed., American Institute of Physics: New York, 1991, p. 444.

91L Lundström, T.: in: Boron-Rich Solids, Proc. 10th Int. Symp. Boron, Borides and Rel. Compounds, Albuquerque, NM 1990 (AIP Conf. Proc. 231), D. Emin, T.L. Aselage, A.C. Switendick, B. Morosin, C.L. Beckel ed., American Institute of Physics: New York, 1991, p. 186.

93B Bolmgren, H., Lundström, T.: J. Alloys Compounds 202 (1993) 73.

94L Lundström, T., Bolmgren, H.: Proc. 11th Int. Symp. Boron, Borides and Rel. Compounds, Tsukuba, Japan, August 22 - 26, 1993, Jpn. J. Appl. Phys. Series 10 (1994), p. 1.

97A Aselage, T.L., Tallant, D.R.: Phys. Rev. B 57 (1997) 2675.

97C Chen, L., Goto, T., Li, J., Aoyagi, E., Hirai, T.: in: Proc. ICT '97, 16th Int. Conf. On Thermoelectrics, A. Heinrich, J. Schumann ed., IEEE: Piscataway, NJ USA, 1997, p. 215.

98A1 Aselage, T.L., Tallant, D.R.: Phys. Rev . B 57 (1998) 2675.

98A2 Aselage, T.L.: J. Mater. Res. 13 (1998) 1786.

Fig. 1.
α-rhombohedral boron structure group. Unit cell volume vs. radius of non-boron element [91L, 93B].

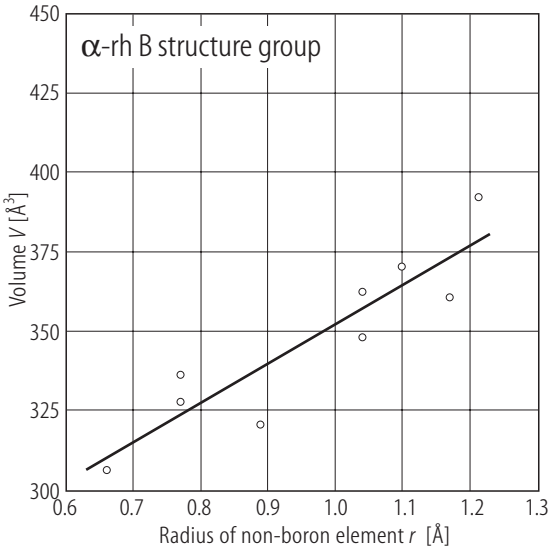

Fig. 2.

Si_4B_{10} = $(B_{12}Si_2)(Si_2)$. Total and partial density of states calculation of the idealized structure [90B]. DOS (Si) for pair and icosahedral sites respectively. DOS (B) for B atoms in B(2) polar sites of the icosahedra (upper curve) and in B(1) equatorial sites of the icosahedra (lower curve).

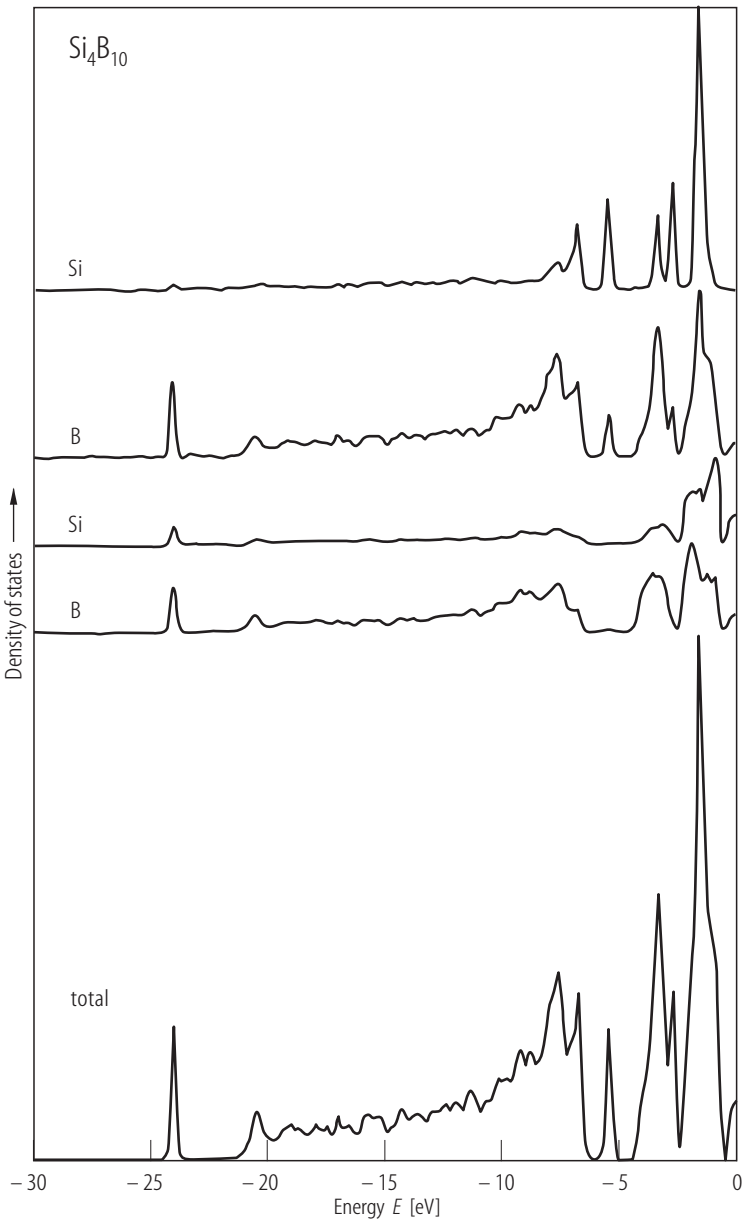

Fig. 3.

SiB_3. Raman spectrum; intensity vs. Raman shift [97A].

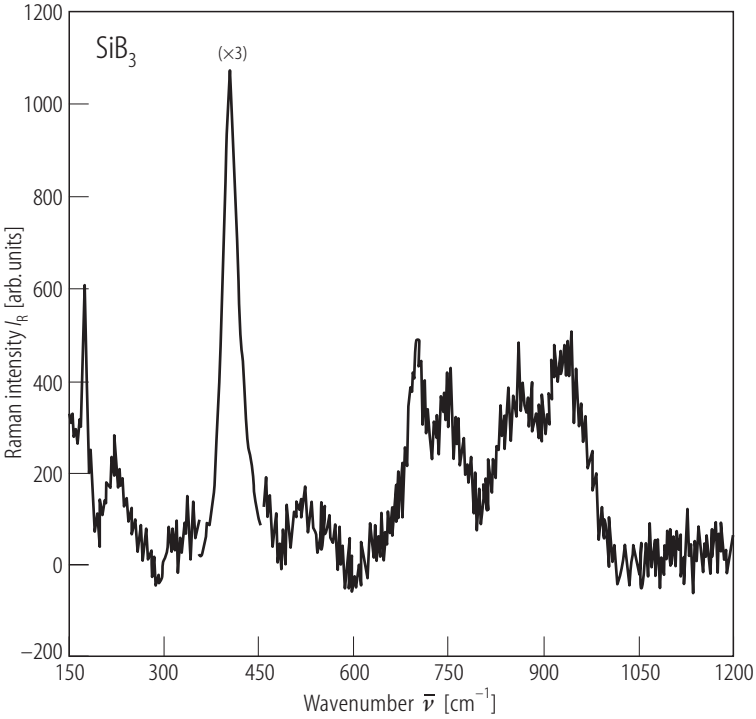

Fig. 4.

$Si_{1-x}B_x$ ($0.05 < x_g < 0.75$). Activation energy of the electrical conductivity vs. temperature. x_g is the boron fraction in the plasma given by $2[B_2H_6]/(2[B_2H_6]+[SiH_4])$ [80P].

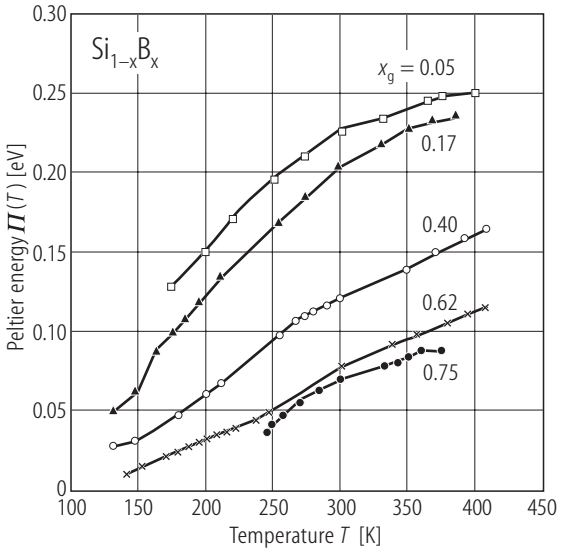

Fig. 5.

$Si_{1-x}B_x$ ($0.05 < x_g < 0.75$). Peltier energy vs. temperature. x_g is the boron fraction in the plasma given by $2[B_2H_6]/(2[B_2H_6]+[SiH_4])$ [80P].

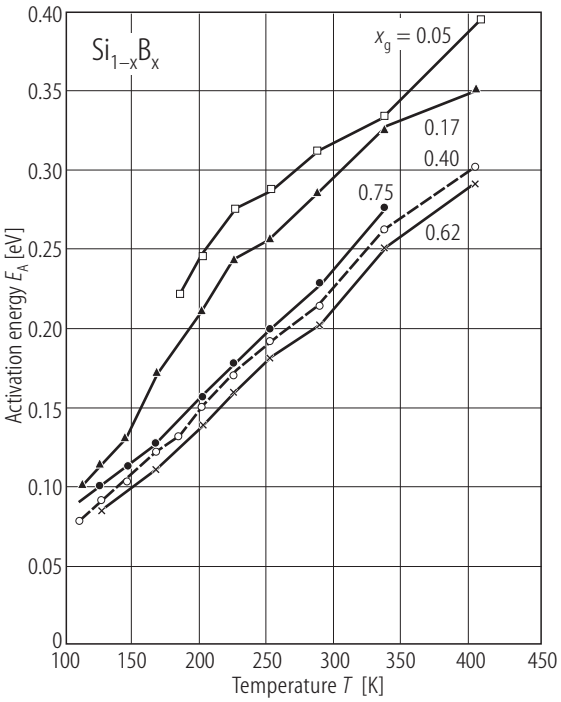

Fig. 6.

$Si_{1-x}B_x$ ($0.05 < x < 1.0$). Density of states $N(E)$, $\sigma(E, 400K)$, and $\sigma(E, T)f(1-f)$ vs. hole energy for the $x_g = 0.17$ film with $W_A = 0.1$ eV (W_A defined by $\mu(E,T) = \mu(E)\exp(W_A/k_BT)$) vs. temperature [80P]. $N(E)$ calculated according to $N(E) = N(E_V) + A\,(E-E_V)$ for $E > E_V$ and $N(E) = N(E_V)\exp[(-B_0(E_V - E)]$ for $E < E_V$ with B_0, tail width of $N(E)$; A, constant, which sets the slope of $N(E)$ above E_V. $\sigma(E)\,f\,(1-f)$ with $f(1-f) = \exp[-(E-E_F)]$ = function of hole energy. For meaning of x_g see caption Fig. 5.

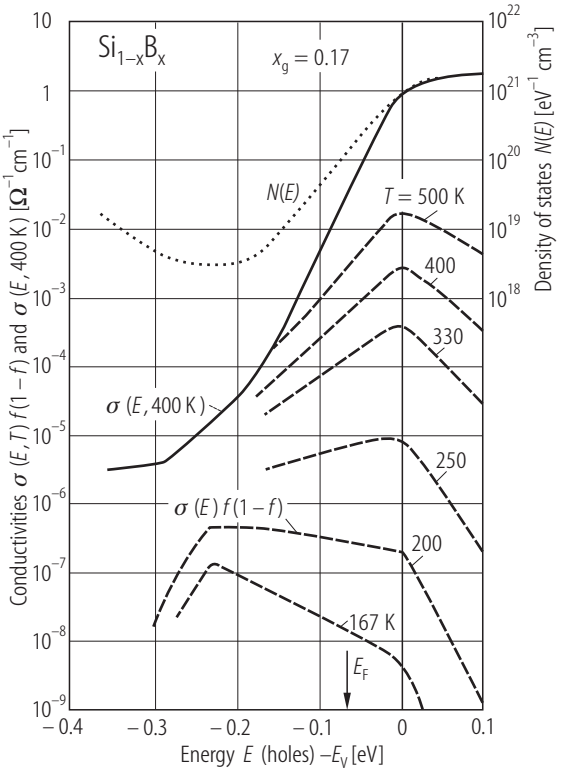

Fig. 7.

SiB_6. Resistivity vs. reciprocal temperature. Results obtained on different samples of material of the same preparation. Sample number 43, results on the same sample obtained in different laboratories [87W], Results from [63F] for comparison.

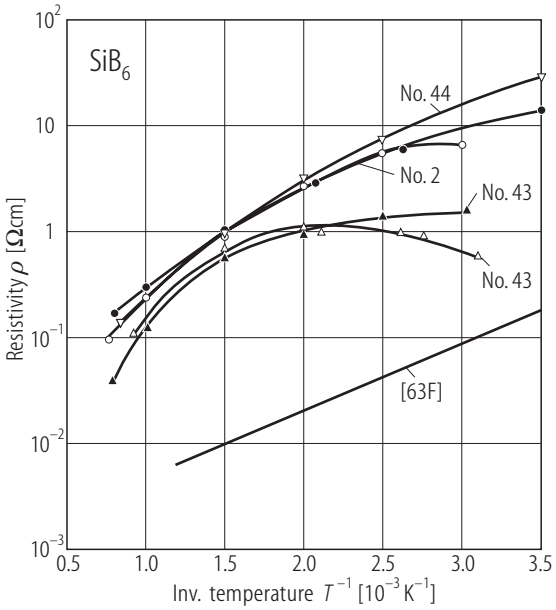

Fig. 8.

SiB_6. Hall data vs. reciprocal temperature. For example: **(a)** sample No. 4; **(b)** sample No. 43 [87W].

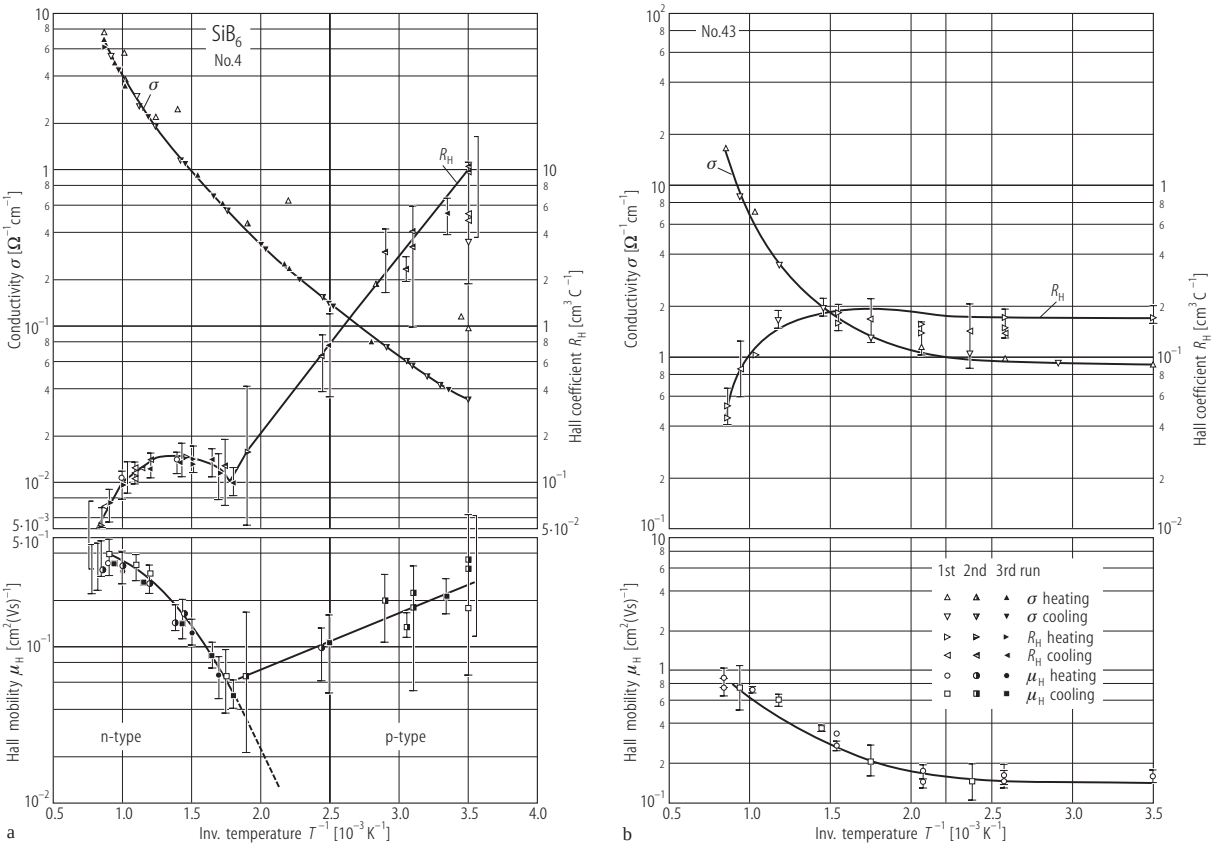

Fig. 9.

SiB_6. Thermoelectric power vs. temperature. Results obtained on different samples of material of the same preparation. Sample number 43, results on the same sample obtained in different laboratories (TECO No. 43 open, full squares; JPL No. 43 open, full circles) [87W].

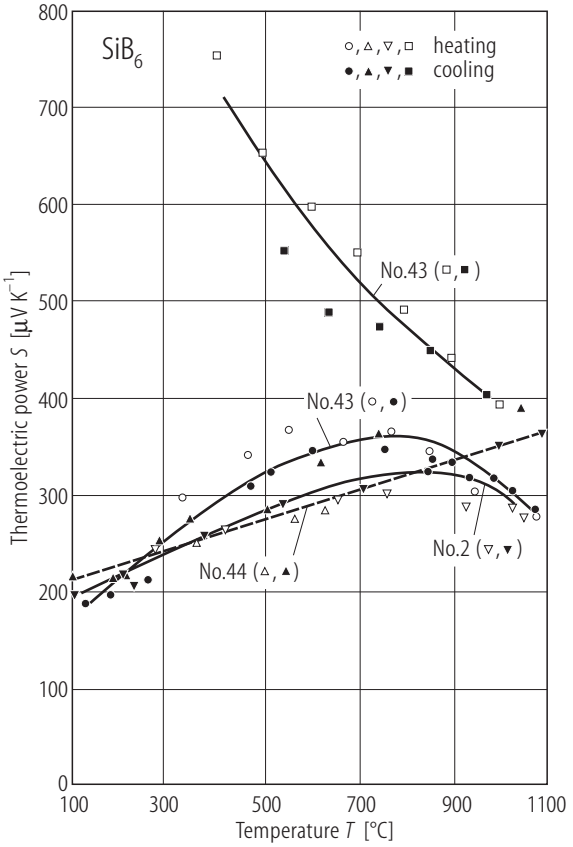

Fig. 10.

a-SiB_6. Raman spectrum; intensity vs. Raman shift [80L].

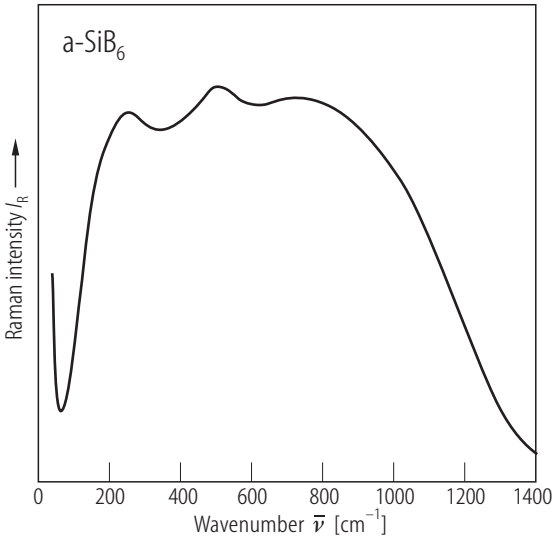

Fig. 11.

SiB_{14}. Electrical conductivity vs. reciprocal temperature [79P].

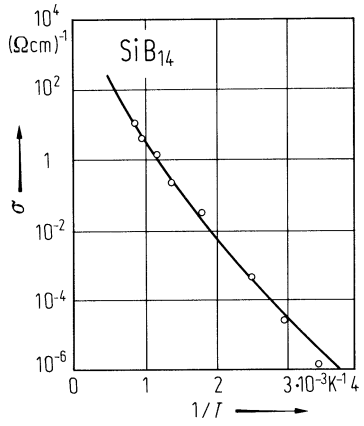

Fig. 12.

SiB_{14}. Thermoelectric power vs. reciprocal temperature [79P].

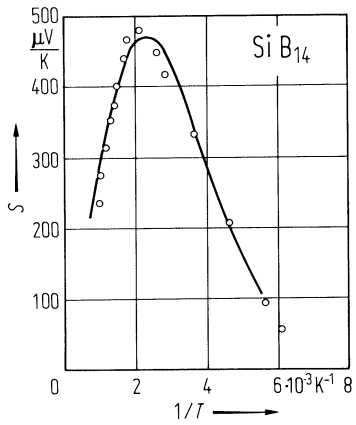

Fig. 13.

SiB_{14}. Conductivity and dielectric constant of polycrystals at various temperatures vs. frequency [78P1].

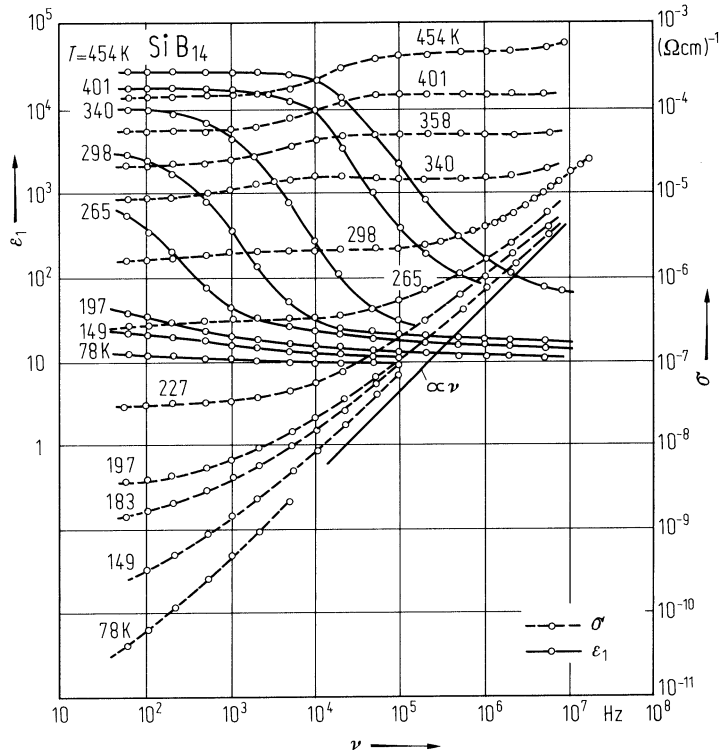

Fig. 14.

SiB_{14}. Cole-Cole diagram. ε_2 vs. ε_1 at various temperatures [791]. The imaginary part ε_2 of the dielectric constant is plotted versus the real part ε_1 with the frequency as parameter. In case of only one relaxation time a half-circle results with its center at $(\varepsilon(0)+\varepsilon(\infty))/2$ on the ε_1 axis. $\varepsilon(0)$ and $\varepsilon(\infty)$ can be taken from the zero crossings of the circle. The maximum value of the half-circle is reached at $\omega = 1/\tau$ (see Fig. 15).

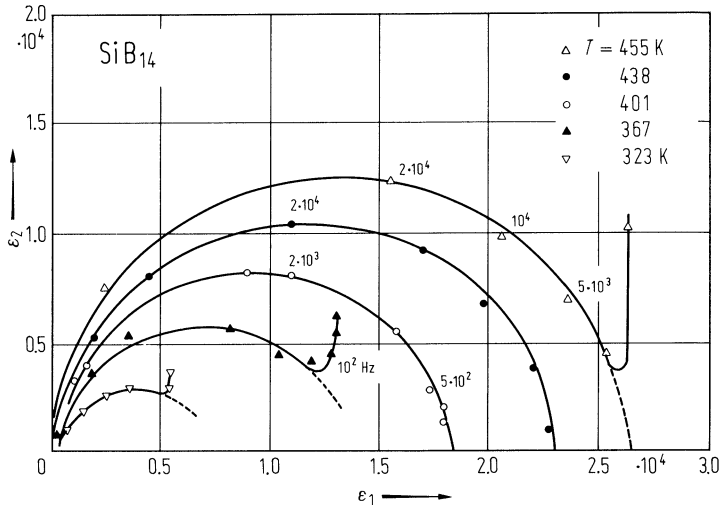

Fig. 15.

SiB_{14}. Relaxation time derived from Cole-Cole diagrams vs. reciprocal temperature [79P].

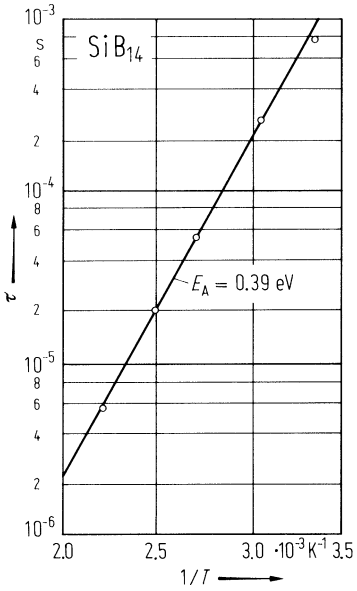

Fig. 16.

Doped B–Si compounds. Resistivity vs. reciprocal temperature (Fe, Co, Ni as doping materials) [81D].

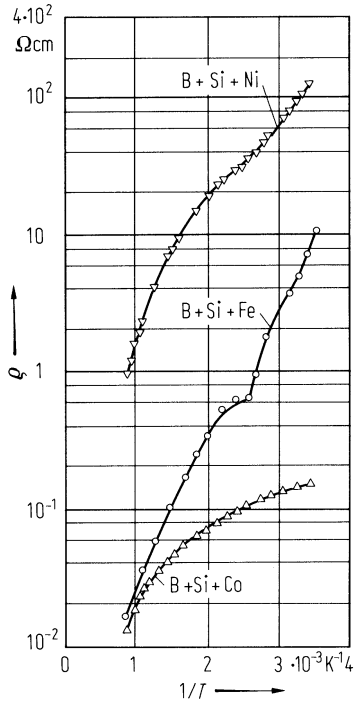

Fig. 17.

Doped B–Si compounds. Thermoelectric power vs. temperature (Fe, Co, Ni as doping materials) [81D].

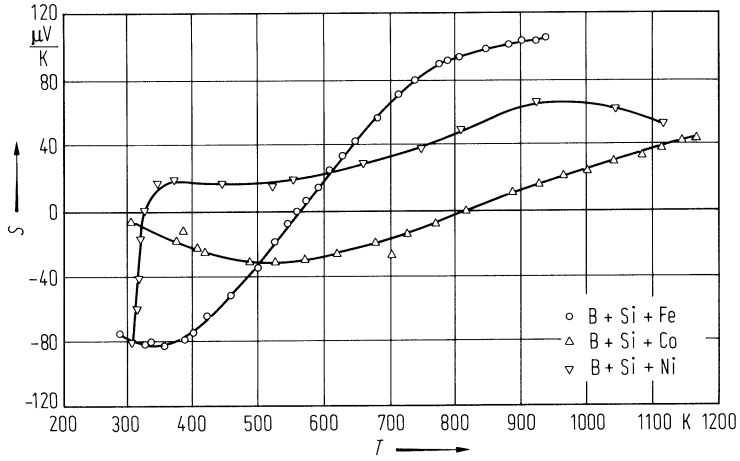

Fig. 18.

a-Si B alloys. Optical energy gap E_{g4} (photon energy at $K = 10^4$ cm^{-1}) and electrical activation energy of anode (A) and cathode (C) deposited films (deposition temperature: 270 ^{0}C) vs. the B fraction in plasma x_g [79T].

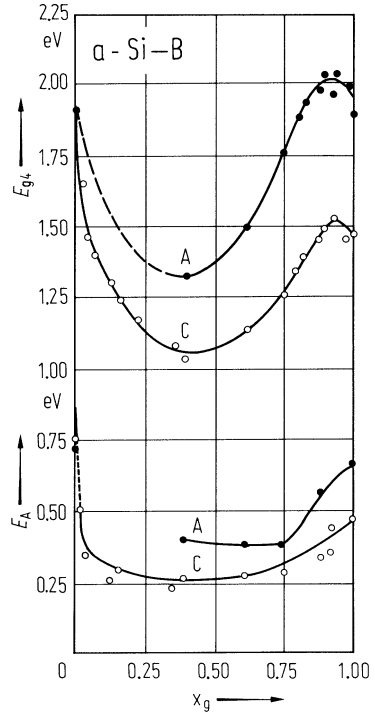

Fig. 19.

a-Si–B alloys. *g*-value and peak-to-peak line-width of ESR signals of samples deposited at 270ºC vs. atomic B fraction in plasma x_g [79T].

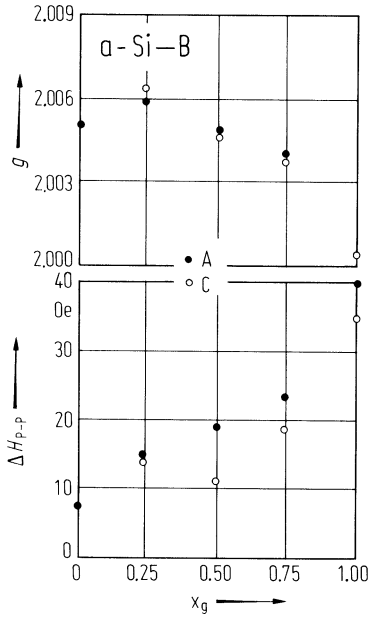

Fig. 20.

a-Si–B alloys. Electrical conductivity of cathode films (deposited at 270°C) vs. reciprocal temperature. Paramter x_g: atomic B fraction in plasma. Dashed curves *b*, *c*, and *d* represent sample *a* after annealing for 30 min at 275, 470 and 570°C, respectively [79T].

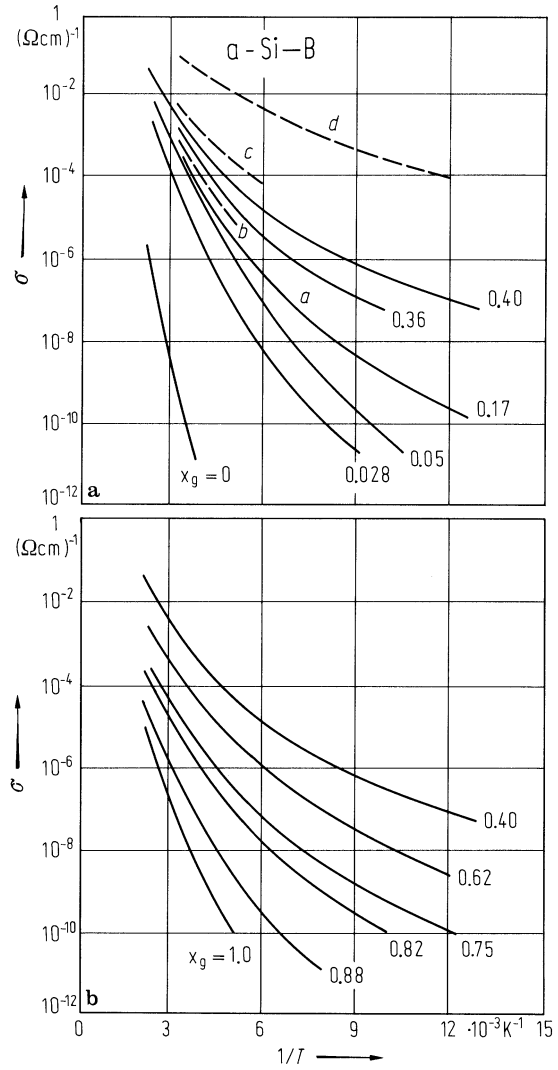

Fig. 21.

a-Si–B alloys. Spin density N_s of anode (A) ane cathode (C) deposited films (deposition temperature 270ºC) vs. B fraction in plasma x_g [79T].

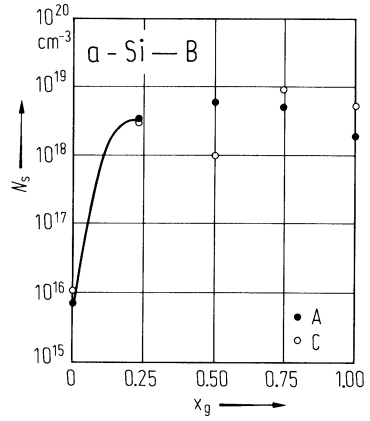

Fig. 22.

a-Si–B alloys. Optical absorption edge of cathode deposited films (deposition temperature: 270ºC) with different B fraction in plasma, x_g. Absorption coefficient vs. photon energy. For further results, see [79T].

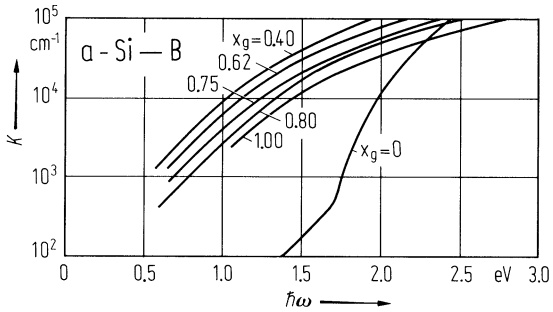

Fig. 23.

a-Si–B alloys. IR transmission of anode deposited films (deposition temperature 25°C) vs. wavenumber. Atomic B fractions x_g = 0; 0.25; 0.5; 0.75; *1*. Film thickness *d* and the transmission measured at (ν/c) = 4000 cm^{-1} are given for each curve. For further results, see [79T].